Waveform Fitting of Cross-Spectra to Determine Phase Velocity Using Aki's Formula

William Menke and Ge Jin
Lamont-Doherty Earth Observatory of Columbia University

Corresponding Author
William Menke, MENKE@LDEO.COLUMBIA.EDU, +1.845.304.5381

Keywords: surface waves, dispersion curves, noise correlation, cross-spectra, Aki's Method

(this paper is not accompanied by an electronic supplement)
(this paper is about 3400 words long and contains 4 figures)

Abstract. A new method is presented for estimating the frequency-dependent phase velocity of ambient noise cross-spectra by waveform fitting of Aki's formula. It employs a three-parameter grid search to determine an initial model, followed by generalized least-squares refinement. The smoothness of the estimated phase velocity is controlled by adjusting a prior variance. In addition to estimating the frequency-dependent phase velocity function, the method calculates its variance and resolution. The method is robust to low noise levels, and so its use may prove especially attractive in cases where short array-deployment times limit the quality of cross-spectral estimates.

Introduction

During the last decade, the development of ambient noise-correlation techniques for reconstructing surface waves propagating between stations has opened up new opportunities for seismic imaging (Shapiro and Campillo, 2004; Shapiro et al. 2005; Calkins et al., 2011). The response of the earth at one seismic station due to a virtual source at another can now be routinely calculated by cross-correlating ambient noise observed at the two stations (Snieder, 2004). While this correlogram contains, in principle, all the usual seismic phases, noise levels have so far limited most studies to Love and Rayleigh waves (surface waves), because they have the highest signal-to-noise ratio. Considerable effort has been put into methods for rapid and accurate computation of the correlograms (Bensen et al., 2007).

At a given period, the path-averaged dispersion function represents the average phase velocity of the surface wave as it propagates from one station to another. In many cases, the propagation path is adequately approximated by the straight-line ray connecting the two stations. Two-dimensional traveltime tomography can then be used to estimate phase velocity as a function of position on the earth's surface, which in turn can be inverted for shear velocity in three three-dimensions. The revolutionary aspect of ambient noise correlation is that the number of rays tends to be much larger, and the spatial and azimuthal coverage of rays tends to be much better, than traditional natural-source methods. The

resulting tomographic images often have sufficiently high resolution to permit detailed structural interpretations.

Another advantage of ambient noise correlation over natural-source methods is the ablity to retrieve the phase velocity at high frequencies. Unlike an earthquake source, the ambient noise virtual source has the best signal-to-noise ratio around the micro-seismic frequency band (~100 mHz). The actual frequency band of ambient noise cross-correlation in which phase velocity is retrievable is also controlled by the interstation distance. The time domain methods usually require interstation spacing being larger than three wavelength for a given period (Bensen et al., 2007), while freuqency domain methods partly work around this limitation and reduce it to 1-2 wavelength (Ekstrom et al., 2009).

A key element of the imaging process is estimating frequency-dependent phase velocity $c(\omega)$ where ω is angular frequency, from the correlograms. As pointed out by Ekstrom et al. (2009), this process can be expedited by working in the frequency domain, since an analytic formula for the cross-spectrum (the Fourier transform of the correlogram) is known (Aki, 1957):

$$\rho(\omega) = A\, J_0\left(\frac{\omega\, r}{c(\omega)}\right) \quad \text{with} \quad A = 1 \tag{1}$$

Here ω is angular frequency and r is inter-station distance. We have added the amplitude factor A to allow for the possibility that an observed cross-spectrum may not be correctly normalized.

Ekstrom et al. (2009) demonstrate that this formula can be used to determined the phase velocity at the frequencies, say $\Omega_\mathrm{i}, i = 1 \cdots N$, at which the cross-spectrum is zero:

$$\text{when } \omega_i = \Omega_\mathrm{i} \quad \text{then} \quad \rho(\Omega_\mathrm{i}) = 0 \quad \text{and} \quad C_i \equiv c(\Omega_\mathrm{i}) = \frac{\Omega_\mathrm{i} r}{Z_{j+k}} \tag{2}$$

Here Z_j is the j-th zero of the Bessel function; that is, $J_0(Z_j) = 0$. Owing to the finite bandwidth of observations, the observed cross-spectrum $\rho^{obs}(\omega)$ is typically measured only for a finite frequency band, and so only a subset of zero-crossings can be estimated. The integer k is introduced to correlate the lowest observed zero of the cross-spectrum with the corresponding zero of the Bessel function. While the value of k is not immediately known, Ekstrom et al. (2009) develop a trial-and-error procedure for determining it, based on prior bounds on the phase velocity; that is, an incorrect value for k leads to an implausible estimate of C_i. Once the phase velocity is known at a sequence of discrete frequencies, its value at other frequencies can be estimated by interpolation.

The most significant limitation of the zero-crossing method is that it performs poorly at high noise levels. Noise causes spurious zeros in $\rho^{obs}(\omega)$, which lead to an erroneous determination of phase velocity. Sometimes, this problem can be recognized because it causes implausible sharp jumps in the estimated phase velocity curve; however, the problem is difficult to correct in an automated way.

Another limitation of the zero-crossing method is on its ability to deal with the station pairs with small interstation distance. For these station pairs, the number of true cross-spectrum $\rho^{obs}(\omega)$ zero-crossing in the interested bandwidth is limited (Figure 4a), hence damaging the accuracy and resolution of the interpolated phase velocity curve after interpolation.

Aki's formula (1) predicts the complete functional form of the cross-spectrum, not just the location of the zero crossings. We show below that additional information about the phase velocity can be determined via "waveform fitting"; that is, determining the phase velocity $c(\omega)$ and amplitude A that match the predicted cross-spectrum $\rho^{pre}(\omega)$ to the observed cross-spectrum, $\rho^{obs}(\omega)$.

Least Squares Estimation of the Cross Spectrum

Our method is based on minimizing the L_2 error,

$$E = \int_{\omega_{min}}^{\omega_{max}} \{\rho^{obs}(\omega) - \rho^{pre}(\omega)\}^2 \, d\omega \tag{3}$$

between the observed cross-spectrum $\rho^{obs}(\omega)$ and the one predicted by Aki's formula, $\rho^{pre}(\omega)$. Here, $(\omega_{min}, \omega_{max})$ is the interested frequency-band of the observations. Additional constraints can be imposed on the minimization, such as $c(\Omega_i) \approx C_i$ (the zero crossing estimates are approximately satisfied), or $d^2c/d\omega^2 \approx 0$ (the phase velocity smoothly varies with frequency), or both. In addition to providing an estimate of phase velocity at all frequencies, as contrasted to just the frequencies of the zero-crossings, this method provides formal estimates of its variance and resolution.

We solve the minimization problem by first approximating the cross-spectrum and phase velocity as frequency series $\boldsymbol{\rho}$ and $\mathbf{c}$, respectively, say with Nvalues and with frequency spacing $\Delta\omega$ between ω_{min} and ω_{max}. The phase velocity $\mathbf{c}$ and amplitude A can be grouped into a model parameter vector $\mathbf{m} = (\mathbf{c}, A)$. Initially, this vector is unknown, but we assume that we have an initial estimate of it, $\mathbf{m}^{(0)} = \left(\mathbf{c}^{(0)}, A^{(0)}\right)$. Ekstrom et al.'s (2009) zero-crossing method could be used to provide this initial estimate; however, in the next section, we put forward an alternative grid-search method that performs especially well at high noise levels.

The data, $\boldsymbol{\rho}^{\mathrm{obs}}$, are assumed to contain noise that is normally-distributed with variance σ_ρ^2. The data equation, $\boldsymbol{\rho}^{\mathrm{obs}} = \boldsymbol{\rho}^{\mathrm{pre}}(\mathbf{m})$, which asserts that the observed and predicted cross-spectra are equal, is non-linear, so we linearize it around an estimate solution $\mathbf{m}^{(\mathrm{p})}$ (with $p = 0$ being the initial estimate). This process leads to the linear equation $\mathbf{G}\,\Delta\mathbf{m} = \Delta\boldsymbol{\rho}$, which links the deviation of the solution from the estimate, $\Delta\mathbf{m} = \mathbf{m} - \mathbf{m}^{(p)}$**,** to the deviation of the data to that predicted by the estimate $\Delta\boldsymbol{\rho} = \boldsymbol{\rho}^{\mathrm{obs}} - \boldsymbol{\rho}^{\mathrm{pre}}\left(\mathbf{m}^{(p)}\right)$. The data kernel $\mathbf{G}$ consists of the derivatives:

$$G_{ij} = \begin{cases} \left.\frac{d\rho_i}{dc_j}\right|_{\mathbf{c}^{(p)},A^{(p)}} = A^{(p)}\,\delta_{ij}\left(\frac{\omega_j r}{\left(c_j{}^{(p)}\right)^2}\right)J_1\left(\frac{\omega_j r}{c_j{}^{(p)}}\right) & \text{for} \quad (1 \le i \le N) \text{ and } (1 \le j \le N) \\ \left.\frac{d\rho_i}{dA}\right|_{\mathbf{c}^{(p)},A^{(p)}} = J_0\left(\frac{\omega_j r}{c_j{}^{(p)}}\right) & \text{for} \quad (1 \le i \le N) \text{ and } j = N+1 \end{cases}$$

(4)

We add two additional linear equations, which represent prior expectations about the phase velocity. The first equation, $\mathbf{m} = \left(\mathbf{c}^{\mathrm{A}}, A^{(0)}\right)$ seeks a model that is close to some prior phase velocity, $\mathbf{c}^{\mathrm{A}}$. This equation serves to keep the estimated phase velocities within a plausible range. We choose a $\mathbf{c}^{\mathrm{A}}$ with a very simple shape - a straight line fit to $\mathbf{c}^{(0)}$ - so not add unnecessary detail into the model. We also assign it very high variance, σ_A^2. The second equation, $\mathbf{Dm} = 0$, imposes smoothness on the phase velocities. Here **D** is the discrete form of the second derivative operator:

$$D_{ij} = \begin{cases} (\Delta\omega)^{-2} & i \le N \text{ and } j = i-1 \\ -2(\Delta\omega)^{-2} & i \le N \text{ and } j = i \\ (\Delta\omega)^{-2} & i \le N \text{ and } j = i+1 \\ 0 & \text{otherwise} \end{cases}$$

(5)

We assign this equation a variance of σ_D^2; the smaller its value, the smoother is the phase velocity curve. The three equations can be grouped into single generalized least squares equation: of the form $\mathbf{F}\,\Delta\mathbf{m} = \mathbf{f}$:

$$\mathbf{F}\,\Delta\mathbf{m} = \begin{bmatrix} \sigma_d^{-1}\mathbf{G} \\ \sigma_A^{-1}\mathbf{I} \\ \sigma_D^{-1}\mathbf{D} \end{bmatrix}\Delta\mathbf{m} = \begin{bmatrix} \sigma_d^{-1}\Delta\boldsymbol{\rho} \\ \sigma_A^{-1}\left(\mathbf{m}^{\mathrm{A}} - \mathbf{m}^{(\mathrm{p})}\right) \\ -\sigma_D^{-1}\mathbf{D}\mathbf{m}^{(\mathrm{p})} \end{bmatrix} = \mathbf{f}$$

(6)

The iterative Generalize Least Squares solution is then obtained by iterating the formulas:

$$\Delta\mathbf{m} = \left(\mathbf{F}^{\mathrm{T}}\mathbf{F}\right)^{-\mathbf{1}}\mathbf{F}^{\mathbf{T}}\mathbf{f} \quad \text{and} \quad \mathbf{m}^{(\mathrm{p}+1)} = \mathbf{m}^{(\mathrm{p})} + \Delta\mathbf{m}$$

with $p = (0, 1, 2, \cdots q)$ until convergence is reached (e.g. Menke, 2012). The covariance of the solution can be approximated as

$$\mathbf{C}_{\mathrm{m}} = \begin{bmatrix} \mathrm{cov}(\mathbf{c}, \mathbf{c}) & \mathrm{cov}(\mathbf{c}, \mathrm{A}) \\ \mathrm{cov}(\mathrm{A}, \mathbf{c}) & \mathrm{cov}(\mathrm{A}, \mathrm{A}) \end{bmatrix} = \left(\mathbf{F}^{\mathrm{T}}\mathbf{F}\right)^{-\mathbf{1}} \tag{7}$$

and the resolution matrix as $\mathbf{R} = \sigma_d^{-2}\left[\sigma_d^{-2}\mathbf{G}^{\mathrm{T}}\mathbf{G} + \sigma_A^{-2}\mathbf{I} + \sigma_D^{-1}\mathbf{D}^{\mathrm{T}}\mathbf{D}\right]^{-1}\mathbf{G}^{\mathrm{T}}\mathbf{G}$.

Grid Search for Initial Solution

The phase velocities of seismic surface waves generally lie within a narrow range of plausible values that are controlled by the shear velocity of the earth's crust and upper mantle, which themselves typically lie with their own narrow range. Furthermore, phase velocity tends to vary smoothly with frequency, reflecting the way in which these long-wavelength waves average earth structure. Consequently, a typical phase velocity curve can be approximated by its values at just a few frequencies, with other values filled in by linear interpolation. This situation makes a grid search an extremely effective way of determining an initial model, which can then be refined by iterative least squares (as described in the previous section).

We begin by defining lower and upper bounds, $\mathbf{c}^{\mathrm{L}}$ and $\mathbf{c}^{\mathrm{U}}$, respectively, between which the phase velocity is presumed to lie. We then define K frequency nodes at which the phase velocity is specified and L values which it can take at each node. We must then search through KL phase velocity curves to find the one with minimum error. Note that we do not need to perform a grid search over amplitude, A, since it can be computed by least squares, once phase velocity is specified:

$$A = [\boldsymbol{\rho}^{\mathrm{pre}}(\mathbf{c}, A = 1)]^{\mathrm{T}}\boldsymbol{\rho}^{\mathrm{obs}} / [\boldsymbol{\rho}^{\mathrm{pre}}(\mathbf{c}, A = 1)]^{\mathrm{T}}\,\boldsymbol{\rho}^{\mathrm{pre}}(\mathbf{c}, A = 1)$$

In order to assess the error of each phase velocity curve, we must linearly interpolate it from K to N frequencies, evaluate $\boldsymbol{\rho}^{\mathrm{pre}}(\mathbf{c}, 1)$ by computing a Bessel function, estimate A by least squares and evaluate the error $E = \mathbf{e}^{\mathrm{T}}\mathbf{e}$ with $\mathbf{e} = \left[\boldsymbol{\rho}^{\mathrm{obs}} - \boldsymbol{\rho}^{\mathrm{pre}}(\mathbf{m})\right]$. The overall computational effort for a single model is modest. It can be further optimized by tabulating the Bessel function, so that only a table-lookup, and not a function call, is required to evaluate it.

We have been successful in performing the grid search on a notebook computer of modest computational capacity for $K \leq 5$ and $L = 40$,. The main requirement of an initial model is not that it fit the cross-spectrum especially well, but that that it fit it without any cycle-skips, so that the least-squares algorithm converges to global minimum. As we show in the example below, the $K = 3$, $L = 40$ case produces initial models that are more than adequate from this perspective.

Example

We apply the method to a dataset of $P = 817$ cross-spectra derived from a combination of land and ocean bottom seismometer stations on and near Papua New Guinea, which were operated for a period of about one and half year starting in March 2010, as part of the CDPAPUA experiment. The cross-spectra were computed by the method described by Ekstrom et al. (2009), and have acceptable signal-to-noise ratio (s.n.r.) in the 0.05 to 0.125 frequency band (N=271 frequencies). This dataset provides an excellent test case, because the region is structurally complex, leading to phase velocity curves with a wide range of shapes, and because it includes examples of both high-quality and low-quality cross-spectra (figure 1). Tomographic images based on the estimated phase velocity curves are presented in (Jin et al. 2014) and are not discussed here.

We perform two sets of grid searches to produce initial estimates of the phase velocity, a three-point grid search with $(K, L) = (3,40)$ and a four-point search with $(K, L) = (4,40)$ (figure 2). In both

cases, we use prior bounds $\mathbf{c}^{\mathrm{L}}$ and $\mathbf{c}^{\mathrm{U}}$ that have a relatively narrow range of 3.2-3.6 km/s at the lowest frequency, widening to 2.75-3.4 km/s at the highest. These choices reflect our belief that the phase velocity curves have normal dispersion and that shallow earth structure, which preferentially affects the higher frequencies, is the most variable. Well-chosen bounds are especially important to prevent cycle-skips in noisiest of the cross-spectra. Comparison of the error reduction of the three-point and four-point searches indicates that former performed nearly as well as the latter (figure 2, A-B); an acceptable initial estimate of phase velocity can be obtained through a three-point grid search.

We have also experimented with a grid search that minimizes an L_1 measure of error, $E = \sum_i |e_i|$, in order to assess whether it leads to better fits, especially for the nosier cross-spectra. Only two code modifications are needed: one in the formula for error, and another to replace the least-squares calculation of the amplitude, A, by one that minimizes the L_1 error. Since this is a one-parameter minimization, we compute A using a steepest-descent method based on the derivative:

$$\frac{dE}{dA} = \frac{d}{dA}\sum_i \left|\rho_i^{obs} - A\rho_i^{pre}\right| = -\sum_i \rho_i^{pre}\,\mathrm{sgn}\left(\rho_i^{obs} - A\rho_i^{pre}\right) \tag{9}$$

Tests indicate that the L_1 method (figure 2, C-D) performs no better than the L_2 method (figure 2, A-B). The L_2 method is preferred since it requires less computational effort.

The initial estimate of the solution is then refined using generalized least squares. The method is dependent upon two ratios, $\varepsilon_1 = \sigma_\rho^2 \sigma_A^{-2}$ and $\varepsilon_2 = \sigma_\rho^2 \sigma_D^{-2}$. The parameter ε_1 controls the deviation of the phase velocity curve from the prior model, and the parameter ε_2 controls its smoothness. After some experimentation, we settled upon $\varepsilon_1 = 0.01$ and $\varepsilon_2 = 50$. While the estimated phase velocity does not depend upon the actual value of the covariance of the cross-spectra, σ_ρ^2, its estimated covariance does. We use a posterior estimate based on the L_2 error of the fit:

$$\sigma_\rho^2 = E/N$$

This variance is used to determine the covariance of the phase velocity, $\mathbf{C}_{\mathrm{m}}$, via the standard error propagation formula (7). The resulting error in the phase velocity, σ_{ρ}, which is in the 0.01 to 0.05 km/s range, corresponds to signal-to-noise ratios in the cross-spectra in the 2:1 to 10:1 range.

The iterative refinement generally leads to only modest (10%) improvement in the fit (figure 2B), but removes the implausible kinks in the phase velocity curves introduced by the simple parameterization of the grid search (figure 4). In a small percentage of cases, the error increased slightly during the refinement. In most of these cases, the increase in error is due to the smoothness condition imposed on the phase velocity curve during the iterative refinement (but not during the grid search); requiring smoothness slightly degrades the quality of the fit. In a few other cases, the solution falls into a local minimum and develops a cycle-slip. The entire estimation process, implemented in MALTAB and including the three-point grid search, took about 2.5 hours on a notebook computer of modest computational power.

Due to the smoothing, the 95% confidence intervals of the estimated phase velocity are very small, about ± 0.02 km/s at a signal-to-noise ratio of 2:1 (figure 4B). The corresponding resolution is poor - about 0.03 Hz – owing to the trading off of resolution and variance that is inherent in all inverse problems (figure 4C-F). A test case (not shown) with $\varepsilon_2 = 5$ led to larger but still acceptable confidence intervals (± 0.03 km/s)) and better resolution (0.01 Hz). However, the estimated phase velocity function contained more detail than the data quality seemed to warrant.

The resolving kernel is bimodal when the target frequency f_0 aligns with a minimum or maximum (extremum) in the cross spectrum (figure 4D). This undesirable shape – a unimodal curve would be preferred - is due to an inherent limitation of this type of inverse problem. The inversion process perturbs the phase velocity, which causes a local stretching or squeezing of the predicted cross-spectrum, allowing it to better fit the observed cross-spectrum. However, the stretching or squeezing has no effect in the

neighborhood of an extremum, since the cross-spectrum is nearly-constant there. The phase velocity at this point is actually being controlled by the quality of the fit to either side.

Discussion and Conclusions

We have described a new method for estimating frequency-dependent phase velocity of cross-spectra of ambient noise by waveform fitting of Aki's (1957) formula. It is an alternative to Ekstrom et al.'s (2009) zero-crossing method, and is based upon a three-parameter grid search followed by generalized least-squares refinement. In addition to estimating the frequency-dependent phase velocity function, the method provides estimates of its variance and resolution. The variance can be used to compute confidence intervals for the phase velocity, which then can be propagated into three-dimensional models of shear velocity.

When applied to high quality cross-spectra (s.n.r. > 10:1), the method is competitive with, but offers no decisive advantage over, Ekstrom et al.'s (2009) zero-crossing method. However, it succeeds even when data quality is poor (s.n.r. ≈ 2:1) and many spurious zero-crossings occur. A method based on identifying the "true" zero-crossings would fail in this case. One such success is illustrated in the low quality test case (figure 2C), where the observed cross-spectrum has 16 zero-crossings, 11 of which are spurious. Waveform fitting also provides more precise dispersion curve than the zero-crossing method when the station spacing is small (Figure 4).

We recommend the method for general use in analyzing ambient noise cross-spectra. It is robust to low noise levels, and so its use may prove especially attractive in cases where short array-deployment times limit the quality of cross-spectral estimates.

Data Sources. Seismic data used in the computation of the cross-spectrum will be available from the Data Management Center of the Incorporated Research Institutions of Seismology under the array code ZN, with a release date of September 2014.

Acknowledgements. This work was supported by the National Science Foundation under grants OCE-0426369 and EAR 11-47742.

References

Aki, K. (1957). Space and time spectra of stationary stochastic waves, with special reference to microtremors, *Bulletin of the Earthquake Research Inst Institute* **35**, 415–457.

Bensen, G. D., M. H. Ritzwoller, M. P. Barmin, A. L. Levshin, F. Lin, M. P. Moschetti, N. M. Shapiro, and Y. Yang (2007). Processing seismic ambient noise data to obtain reliable broad-band surface wave dispersion measurements, *Geophysical Journal International* **169**, 1239-1260, doi: 10.1111/j.1365-246X.2007.03374.x.

Calkins, J. A., G. A. Abers, G. Ekstrom, K. C. Creager, and S. Rondenay (2011). Shallow structure of the Cascadia subduction zone beneath western Washington from spectral ambient noise correlation, *Journal Geophyical Research - Solid Earth* **116**, doi: 10.1029/2010jb007657.

Ekström, G., G.A. Abers and S.C. Webb (2009). Determination of surface-wave phase velocities across USArray from noise and Aki's spectral formulation, *Geophysical Research Letters* **10**, DOI: 10.1029/2009GL039131

Menke, W. (2012). *Geophysical Data Analysis, Discrete Inverse Theory, MATLAB Edition*, Elsevier, New York, 293pp.

Shapiro, N. M., and M. Campillo (2004). Emergence of broadband Rayleigh waves from correlations of the ambient seismic noise, *Geophysical Research Letters* **31**, doi: 10.1029/2004gl019491.

Shapiro, N. M., M. Campillo, L. Stehly, and M. H. Ritzwoller (2005). High-resolution surface-wave tomography from ambient seismic noise, *Science* **307**, 1615–1618.

Snieder, R. (2004). Extracting the Green's function from the correlation of coda waves: A derivation based on stationary phase, *Physical Review E* **69**, doi: 10.1103/PhysRevE.69.046610.

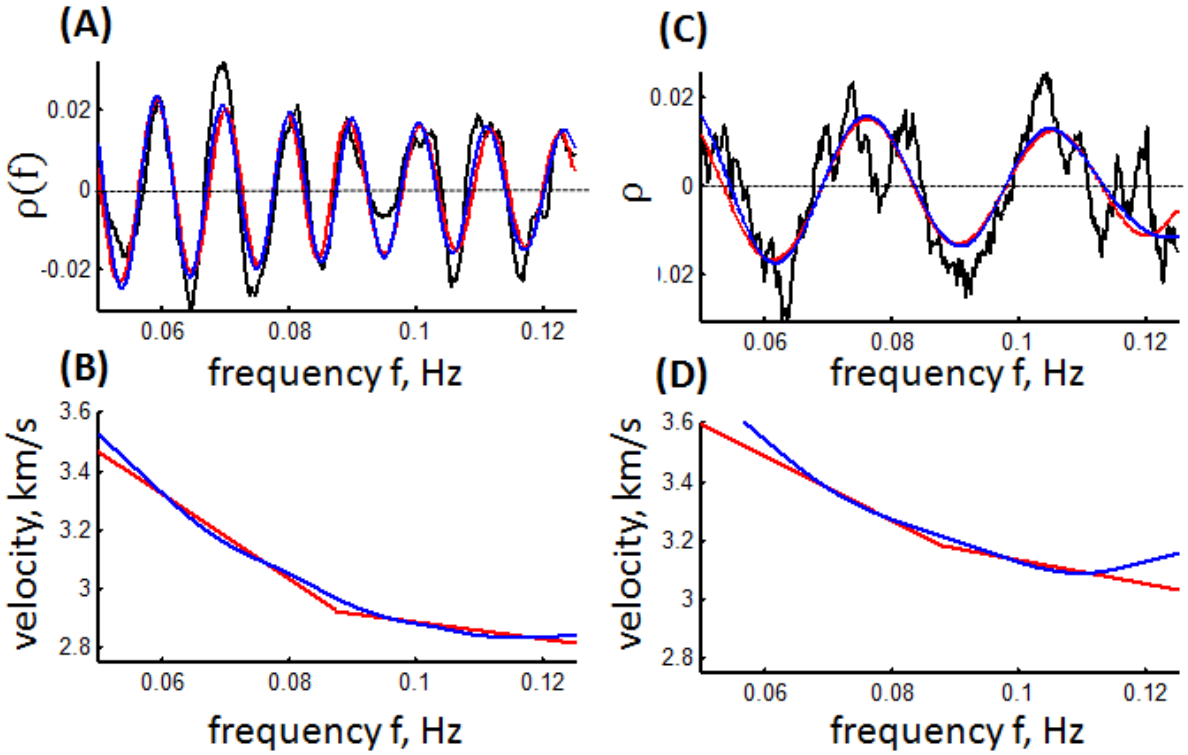

Fig. 1. (A) High-quality data (s.n.r. of 10:1) (black), with prediction of three-point grid search for solution with minimum L_2 error (red) and least-squared refinement (blue). (B) Corresponding estimated phase velocity curves. (C-D) Same as A-B, but for lower quality data (s.n.r. of 2:1).

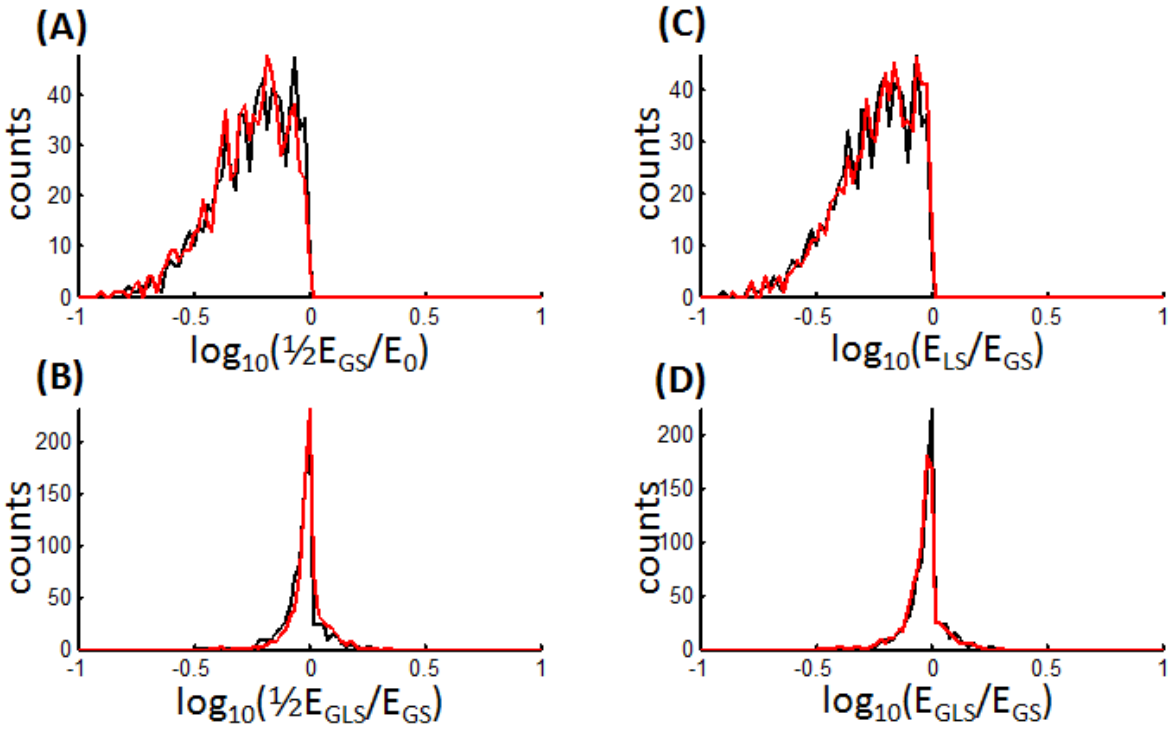

Fig. 2. Histograms of prediction error. (A) L_2 error E_{GS} of the three-point grid search (black) and four-point grid search (red) normalized by the power E_0 in the cross-spectrum. (B) Error E_{GLS} of the generalized least squares refinement, normalized by the grid search error E_{GS}, where the results of three-point grid search (black) and four-point grid search (red) were used as starting models. (C-D) Same as A and B, except L_1error is minimized in the grid search.

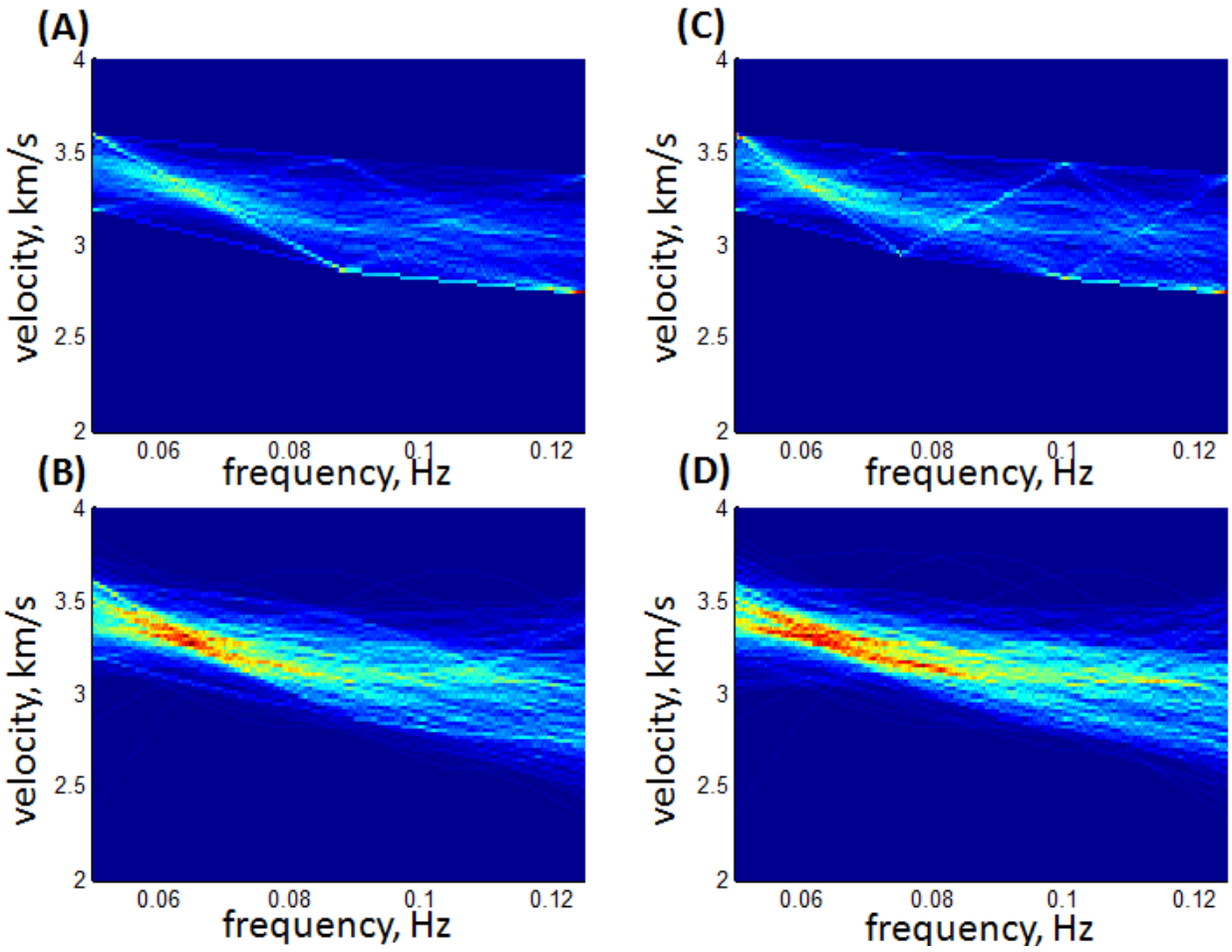

Fig. 3. Histograms of estimated phase velocity, $c(f)$, as a function of frequency, f. (A) Three-point grid search with L_2 measure of error. (B) Least-squares refinement of three-point grid search. (C-D) Same as A-B, but for four-point grid search. Red colors correspond to the highest density of phase velocity measurements.

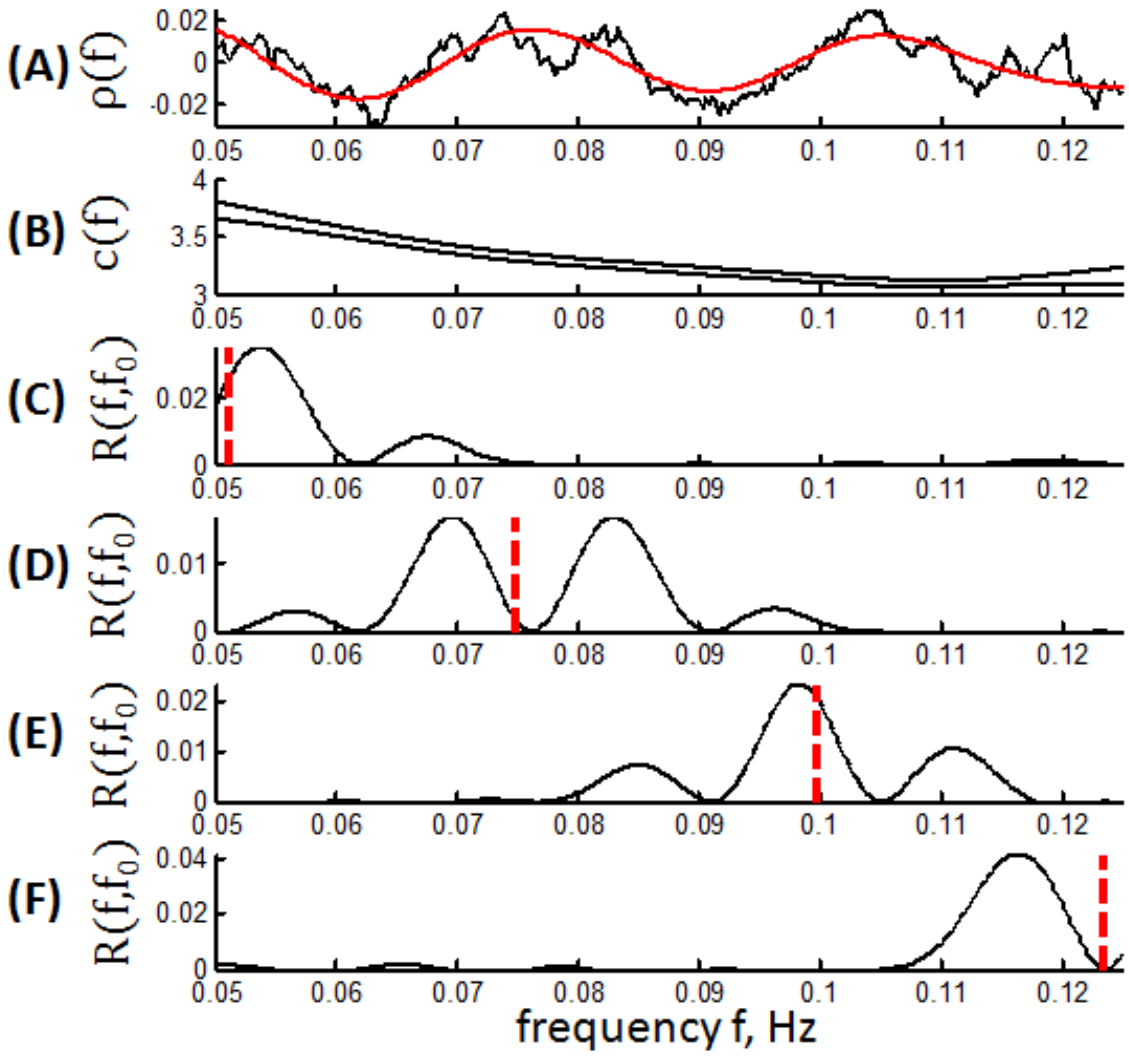

Fig. 4. Variance and resolution of estimated phase velocity curves. (A) Observed (black) and predicted cross-spectrum, $\rho(f)$ (red). (B) 95% confidence limits of estimated phase velocity, *c(f)*. (C-F) Resolving kernels, $R(f, f_0)$ (black), for estimated phase velocity for selected target frequencies, f_0 (red bars).